

Characterizing multi-mode nonlinear dynamics of nanomechanical resonators

Ata Keşkekler*,¹ Vincent Bos,¹ Alejandro M. Aragón,¹ Peter G. Steeneken,^{1,2} and Farbod Alijani*¹

¹*Faculty of Mechanical, Maritime and Materials Engineering,
Delft University of Technology, Mekelweg 2, 2628 CD Delft, The Netherlands*

²*Kavli Institute of Nanoscience, TU Delft, The Netherlands*

(Dated: April 5, 2023)

Mechanical nonlinearities dominate the motion of nanoresonators already at relatively small oscillation amplitudes. Although single and coupled two-degrees-of-freedom models have been used to account for experimentally observed nonlinear effects, it is shown that these models quickly deviate from experimental findings when multiple modes influence the nonlinear response. Here, we present a nonlinear reduced-order modelling methodology based on FEM simulations for capturing the global nonlinear dynamics of nanomechanical resonators. Our physics-based approach obtains the quadratic and cubic nonlinearities of resonators over a wide frequency range that spans 70 MHz. To qualitatively validate our approach, we perform experiments on a graphene nanodrum driven opto-thermally and show that the model can replicate diverse ranges of nonlinear phenomena, including multi-stability, parametric resonance, and different internal resonances without considering any empirical nonlinear fitting parameters. By providing a direct link between microscopic geometry, material parameters, and nonlinear dynamic response, we clarify the physical significance of nonlinear parameters that are obtained from fitting the dynamics of nanomechanical systems, and provide a route for designing devices with desired nonlinear behaviour.

Nanomechanical resonators are the devices of choice for high-performance sensing since they respond to minuscule forces [1–3]. More recently, they have emerged as ideal systems for exploring nonlinear dynamic phenomena. Thanks to their high force sensitivity they are easily driven into the nonlinear regime [4]. Their small mass leads to high resonance frequencies, which facilitates high-speed measurements and, especially in ultrathin resonators, the high aspect ratio allows tuning of tension and resonance frequencies to explore a variety of nonlinear phenomena [5].

When nanomechanical devices are driven into resonance, already at small amplitudes Duffing nonlinearities precipitate in the motion, leading to softening- or hardening-type nonlinear responses [6]. When the nonlinear regime is traversed further, with the increase in drive amplitude, other eigenmodes begin to partake in the motion through autoparametric excitations and nonlinear intermodal couplings [7]. In this nonlinear domain, many studies have reported significant impact of these nonlinear couplings on the effective dissipation and stiffness of the vibration modes [8, 9]. A number of exotic nonlinear phenomena have also been showcased, ranging from frequency noise suppression [10] and intermodal storage of mechanical energy [11, 12], to the generation of mechanical frequency combs [13, 14].

Efforts made to date in explaining nonlinear phenomena often rely on proposing analytical nonlinear low-degrees-of-freedom (DOFs) models that are fit to the experimen-

tal data to prove their validity. However, since there is no direct link between the magnitude of the resulting fit parameters and the geometry or material properties of the nanomechanical device, it is difficult to evaluate whether these models are the only ones that can account for the experimental data, and which parameters are the most relevant. Moreover, since there is no direct link between the model parameters and the underlying physics, it is difficult to extract device information from the fitting. A realistic description of the complex nonlinear dynamics of nanoresonators with pure analytical methods such as rotating-wave approximation [15] or harmonic balancing [16] is not always sufficiently accurate, because analytical methods are constrained to a limited number of DOFs. Purely numerical methods such as molecular dynamics or dynamic nonlinear Finite Element Method (FEM) simulations may resolve this issue, yet they are computationally expensive [17, 18] and provide less insight. Therefore, an intermediate approach, whereby analytical multi-mode nonlinear dynamic models are constructed from the physical device properties using numerical methods, can be extremely valuable for the precise and fast analysis of the nonlinear dynamics of nanomechanical systems.

In this article we develop and utilize a physics-based Reduced-Order Model (ROM) to characterize multi-mode nonlinear dynamics of nanomechanical resonators over a wide frequency range. Our approach makes use of FEM simulations to probe the geometric nonlinearities of nanoresonators for a large number of coupled vibrational modes. To validate our method, we perform experiments on a graphene nanodrum that is driven opto-thermally into the strong mode coupling regime. We show that the physics-based model can capture the response of the seven directly excited and two parametrically excited

*Corresponding authors:

Ata Keşkekler <a.keskekler-1@tudelft.nl>,

Farbod Alijani <f.aliyani@tudelft.nl>

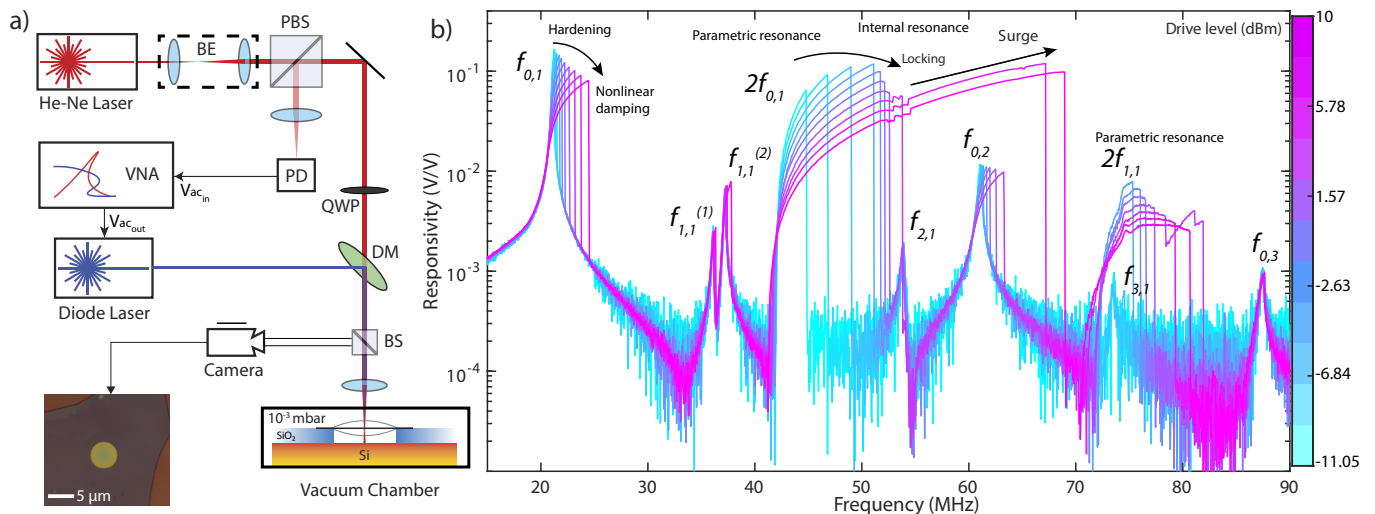


FIG. 1: Measuring the motion of a nonlinear graphene nanodrum. (a) Schematic of the measurement setup. BE, PBS, BS, QWP, DM and VNA stand for beam expander, polarized beam splitter, beam splitter, quarter-wave plate, dichroic mirror and vector network analyzer, respectively. (b) Measurements reveal a range of nonlinear dynamic phenomena for the graphene nanodrum at relatively small amplitudes. At high drive levels, graphene nanodrum exhibits complex nonlinear behavior where the frequency response shows hardening nonlinearity, signatures of nonlinear damping, parametric resonance, mode couplings and internal resonances. The labels $f_{p,m}$ are frequencies associated with circular drum mode shapes that are found from FEM simulations. Here, p stands for the number of nodal lines and m is the number of nodal circles.

modes of the graphene nanodrum from linear to nonlinear regime, in a frequency range that spans 70 MHz. The model uses the Young’s modulus and pre-stress to obtain the coupling coefficients, thus providing insight into the influence of geometric and physical parameters on the coupled dynamics of nanomechanical resonators. Since the method is FEM-based, it can be applied further to nanomechanical devices of virtually any geometry, allowing predicting and designing a variety of nonlinear phenomena.

As an experimental model system for demonstrating the method, we probe the complex dynamics of a graphene nanodrum resonator. The resonator is fabricated by dry transfer of $h = 10$ nm thick multi-layer graphene over a $d = 5 \mu\text{m}$ diameter and 285 nm deep circular cavity, etched in a layer of SiO_2 on a Si substrate. To study the mechanical vibrations of the nanodrum, we optothermally drive it using a blue laser ($\lambda = 405$ nm) and measure its response by a red laser ($\lambda = 633$ nm) using laser interferometry (Fig. 1a). At low drive powers, a linear set of resonance peaks can be obtained, showing the activation of multiple modes of vibration that we can identify easily using FEM simulations. As the drive level is increased, the nanoresonator quickly shows signs of nonlinearity (Fig. 1b). It is possible to observe the well-studied Duffing (hardening type) nonlinearity in several modes already at relatively small amplitudes (below -6 dBm).

By further increasing the drive level, we notice rapid activation of a plethora of nonlinear dynamic responses. For instance, when the excitation frequency is tuned to twice

the resonance frequency of the modes $f_{0,1}$ and $f_{1,1}$, it is possible to detect strong parametric resonances [19]. Since the tension of the nanodrum is directly related to its stiffness, modulation of the tension via opto-thermal actuation parametrically excites the nanodrum. Consequently, for conditions where the drive is strong enough, period doubling instabilities emerge, resulting in parametric resonances [19]. These resonances can reach high amplitudes and span wide frequency ranges thanks to the Duffing hardening nonlinearity. Especially at drive frequencies where the frequencies of these modes satisfy internal resonance conditions [7], they strongly interact with other modes of vibration. This can be observed in Fig. 1b at drive levels above 2 dBm, around the region where the parametrically driven $f_{0,1}$ and the directly driven $f_{2,1}$ are interacting. As the parametric response of $f_{0,1}$ approaches $f_{2,1}$, it is also possible to observe a decrease in the responsivity as well as a reduction in the rate of increase in the nonlinear frequency of the parametric resonance – a phenomenon that we label as “locking” in Fig. 1b. Only after a certain drive level is reached, this “locking” barrier is surpassed, and the parametric resonance surges to a higher amplitude and frequency [9]. Other than this apparent interaction, a similar coupled dynamic response can be noticed in the neighborhood of the parametrically driven $f_{1,1}$ and directly driven $f_{3,1}$.

Another interesting observation is the decrease in the responsivity of the nanoresonator for the directly driven modes of vibration with the increase in drive level (see the nonlinear response around $f_{0,1}$ and $f_{0,2}$ in Fig. 1b for instance). This reduction, which is a result of the emer-

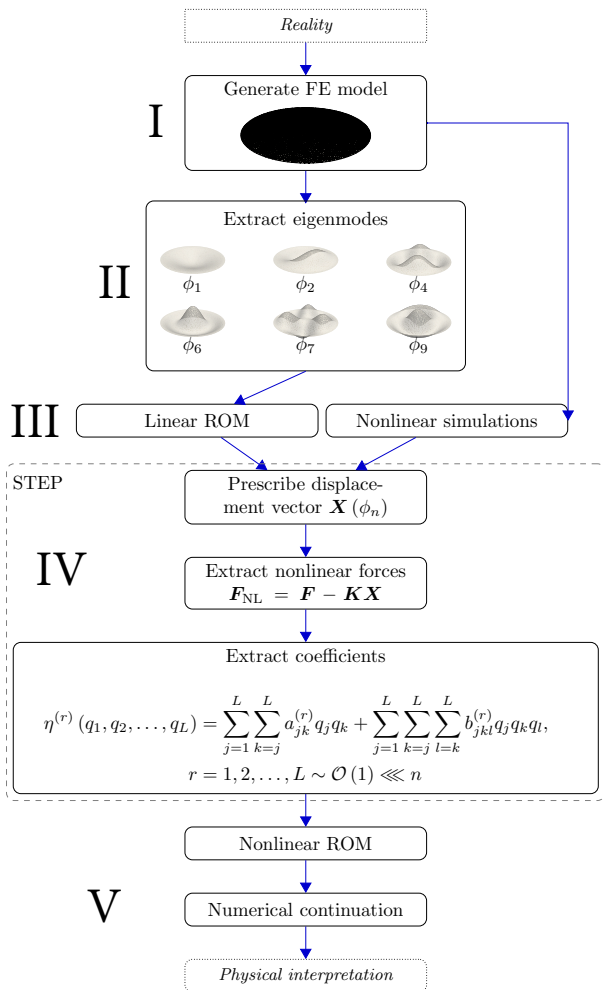


FIG. 2: The flowchart of the ROM procedure for nonlinear dynamic simulations. The frequency response and AFM measurements are used to extract the physical parameters for building the FE model, which is then utilized to obtain linear and nonlinear reaction forces of the device, given prescribed displacements in terms of superposition of eigenmodes. These forces are then used for extracting the coefficients of nonlinear terms in the ROM [21]. Finally the nonlinear multi-mode model is simulated numerically to obtain the full nonlinear dynamic response.

gence of nonlinear dissipation [6], was first observed in resonators that can reach strong nonlinear regime [20]. It was recently shown that such nonlinear dissipation process could also be mediated when two modes of vibration are coupled via internal resonance [9]. Capturing such nonlinear dissipation processes by analytical means, however, when multiple modes are contributing to the response, is far from being trivial. In order to deepen our understanding of these complex multi-modal interactions, we thus introduce a FEM-based ROM model [21]. The method for modelling the complex dynamics showcased in Fig. 1b consists of five steps, starting with the

generation of a FEM model of the nano device (step I in Fig. 2). For this purpose, any FEM software package that can handle geometric nonlinearities can be used (we have chosen to use COMSOL in this work). The FEM model of the circular graphene nanodrum resonator uses plate elements and fixed boundary condition. We use the literature values for the mass density and Poisson's ratio of graphene to be $\rho = 2267 \text{ kg m}^{-3}$ and $\nu = 0.16$. As the geometry of the resonator is already known from optical microscopy and Atomic Force Microscopy (AFM) measurements, this leaves only two unknown parameters to be determined for building the model, namely the pre-tension and the Young's modulus of the nanodrum. Since the linear resonance frequencies of the graphene membrane are dominated by the pre-tension, we can extract its value from frequency response measurements at low drive levels. However, if only the fundamental frequency is taken into account when determining the pre-tension, it is not possible to explain the splitting of the asymmetric modes, like $f_{1,1}^{(1)}$ and $f_{1,1}^{(2)}$ in Fig. 3a. In a perfectly symmetric drum, these eigenmodes are degenerate, i.e., they have the same frequency. But in practice, there is a mismatch in the tension along the in-plane axes that causes these modes to have slightly different frequencies. The frequencies of the first degenerate mode, together with the fundamental frequency, are enough to extract the tension in the membrane by matching the experimental linear resonance frequencies of the first three modes in the FEM analysis. By doing this we found the pre-tension in the membrane to be $T_x = 0.321 \text{ N m}^{-1}$ and $T_y = 0.257 \text{ N m}^{-1}$ for two perpendicular axes in the plane. To find Young's modulus of the graphene nanodrum we then used the linear resonance frequencies of the higher modes following the method described in [22]; we found a Young's modulus of 410 MPa (Fig. 3a), which is within the values reported in the literature [23, 24].

By performing linear vibration analysis in the FEM software, we can now obtain the $n \times n$ linear mass and stiffness matrices (\mathbf{K} and \mathbf{M} , respectively), as well as the eigenvalues ω_n and eigenmode matrix Φ , where n is the number of DOFs used in the FEM simulations (step II in Fig. 2). Therefore, for an n -dimensional displacement vector \mathbf{X} in the FEM model, we obtain the following set of discrete equations:

$$\mathbf{M}\ddot{\mathbf{X}}(t) + \mathbf{C}\dot{\mathbf{X}}(t) + \mathbf{K}\mathbf{X}(t) + \mathbf{H}(\mathbf{X}(t)) = \mathbf{F}(t), \quad (1)$$

where $\ddot{\mathbf{X}}$ denotes acceleration, $\dot{\mathbf{X}}$ velocity, \mathbf{H} the nonlinear force vector, and $\mathbf{F}(t)$ is the nodal force vector. Here, the linear damping matrix \mathbf{C} accounts for dissipation. Currently nonlinear damping is not yet included in the equation of motion, although viscous material damping might be added via an imaginary term in the material's Young modulus. Evidently, in a finely meshed FEM model, the large number of degrees of freedom n in Eq. (1) in combination with the wide frequency range,

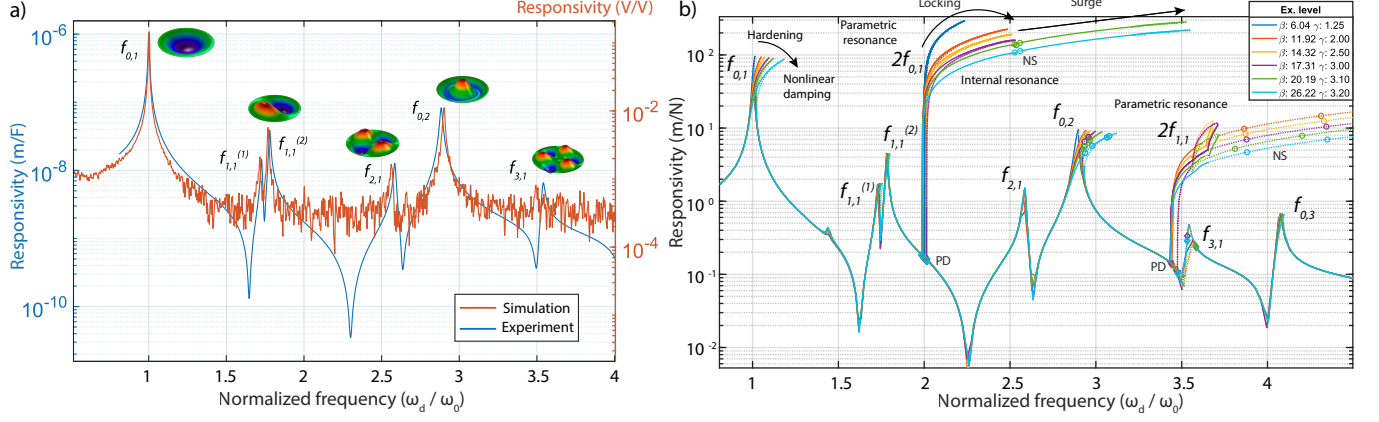


FIG. 3: The simulated linear and nonlinear dynamic responses of the ROM. a) Frequency response measurements at linear regime are used for extracting the pre-tension and Young's Modulus of the membrane. b) The simulated nonlinear frequency response of the graphene nanodrum, where β is the direct drive intensity and γ is the parametric drive intensity. It is possible to capture the experimentally observed nonlinear phenomena using the ROM, such as hardening nonlinearities, parametric resonances and internal resonance induced physics such as frequency locking and amplitude surge. Bifurcation points are also detected during numerical simulations, diamond indicators stand for period doubling bifurcations (PD), whereas circles stand for the Neimark-Sacker bifurcation (NS).

makes it practically impossible to use the FEM for simulating nonlinear dynamic responses like those in Fig. 1b. Therefore, we use a subset L of the n eigenmodes for explaining the observed physics, where $L \ll n$. This mathematically means reducing the number of DOFs to only a few that are capable of replicating the nonlinear dynamics of the full model. To do so, we use the modal coordinate transformation $\mathbf{X} = \Phi \mathbf{q}$, expressing the displacement as a superposition of eigenmode shapes, and only select a subset $\Phi_{n \times L}$ of eigenvectors, such that \mathbf{q} is the L -dimensional modal amplitude vector. Using this transformation, Eq. (1) can be re-written in modal coordinates as

$$\tilde{\mathbf{M}}\ddot{\mathbf{q}}(t) + \tilde{\mathbf{C}}\dot{\mathbf{q}}(t) + \tilde{\mathbf{K}}\mathbf{q}(t) + \boldsymbol{\eta}(\mathbf{q}(t)) = \tilde{\mathbf{F}}(t), \quad (2)$$

where $\tilde{\mathbf{M}} = \Phi^T \mathbf{M} \Phi$, $\tilde{\mathbf{C}} = \Phi^T \mathbf{C} \Phi$, $\tilde{\mathbf{K}} = \Phi^T \mathbf{K} \Phi$, $\boldsymbol{\eta} = \Phi^T \mathbf{H}$ and $\tilde{\mathbf{F}}(t) = \Phi^T \mathbf{F}(t)$.

From the linear FEM eigenmode simulation, all these matrices and vectors except $\boldsymbol{\eta}$ can be determined (step I-III in Fig. 2). To obtain this nonlinear matrix we perform multiple nonlinear stationary FEM simulations, with suitably chosen displacements \mathbf{X}_c along the Stiffness Evaluation Procedure (STEP, see IV in Fig. 2) that we briefly outline in what follows and along the lines of Ref. 21.

For any nodal displacement vector $\mathbf{X} = \mathbf{X}_c$, the reaction forces can be transformed into the modal domain and used for the extraction of nonlinear internal forces of the nanodrum. We do this by carefully prescribing nodal displacement vectors \mathbf{X}_c , to calculate the corresponding linear reaction forces \mathbf{F}_L since $\mathbf{F}_L = \mathbf{K} \mathbf{X}_c$. After finding the linear reaction forces, we perform a full nonlinear

static analysis in the FEM package, considering that the nanodrum is subjected to the same displacement vector \mathbf{X}_c , and obtain the total nodal reaction force \mathbf{F}_T . By subtracting the linear reaction forces from this full static solution, i.e., $\mathbf{F}_{NL} = \mathbf{H}(\mathbf{X}_c) = \mathbf{F}_T(\mathbf{X}_c) - \mathbf{K} \mathbf{X}_c$, we then obtain the nonlinear reaction force and map that on the subset of eigenmodes selected as follows: $\boldsymbol{\eta} = \tilde{\mathbf{F}}_{NL} = \Phi^T \mathbf{F}_{NL}$ (see steps III and IV in Fig. 2). We finally expand this nonlinear reaction force for every mode of vibration in terms of quadratic and cubic nonlinear terms as follows:

$$\eta^{(r)} = \sum_{j=1}^L \sum_{k=j}^L \alpha_{jk}^{(r)} q_j q_k + \sum_{j=1}^L \sum_{k=j}^L \sum_{l=k}^L b_{jkl}^{(r)} q_j q_k q_l, \quad (3)$$

where r stands for the r th equation of motion also associated with the r th mode, and j, k, l are the mode numbers. Furthermore, L is the number of modes that is being considered in the ROM. We note that these cubic and quadratic nonlinear terms for single or two-mode models are commonly used to simulate nonlinear dynamics of nanomechanical resonators. However, here we extract them purely from geometric nonlinearities and can expand that to any number of modes of vibration, up to the number of DOFs that is being considered in the FEM simulations.

The procedure explained above enables us to generate a set of linearly independent F_{NL} equations by applying different displacement vectors $\mathbf{X}_c(\phi_r)$, $r = \{1, \dots, L\}$; these are selected such that they are superpositions of eigenvectors ϕ_r where each combination provides unique information about a nonlinear term through simulations, e.g., $\mathbf{X}_c = \pm \phi_j q_j \pm \phi_k q_k \pm \phi_l q_l$. In order to obtain information about the nonlinear reaction forces, the modal

amplitudes in the displacement vector \mathbf{X}_c should be chosen such that the nano device reaches the geometric nonlinear regime.

To clarify the procedure outlined above, we demonstrate how the nonlinear coefficients of the ROM can be derived for two hypothetical generalized coordinates, q_1 and q_2 . We start by determining the uncoupled nonlinear coefficients of the system. For the first generalized coordinate q_1 , we construct displacement vectors \mathbf{X}_c from ϕ_1 , such that only nonlinear terms associated with q_1 are activated:

$$\mathbf{X}_1 = +\phi_1 q_1, \quad (4)$$

$$\mathbf{X}_2 = -\phi_1 q_1. \quad (5)$$

This results in two equations with two unknowns:

$$\tilde{\mathbf{F}}_{\text{NL}}^{(1)}(\mathbf{X}_1) = \alpha_{11}^{(1)} q_1^2 + b_{111}^{(1)} q_1^3, \quad (6)$$

$$\tilde{\mathbf{F}}_{\text{NL}}^{(1)}(\mathbf{X}_2) = \alpha_{11}^{(1)} q_1^2 - b_{111}^{(1)} q_1^3, \quad (7)$$

which can be solved to obtain $\alpha_{11}^{(1)}$ and $b_{111}^{(1)}$, that are namely the quadratic and cubic uncoupled nonlinear terms for the modal coordinate q_1 . Similarly, by prescribing the system to move on its second eigenmode ϕ_2 we can obtain $\alpha_{22}^{(2)}$ and $b_{222}^{(2)}$. Next, in order to determine the coupled terms, we use the superposition of the eigenmodes as follows:

$$\begin{aligned} \mathbf{X}_3 &= +\phi_1 q_1 + \phi_2 q_2, \\ \mathbf{X}_4 &= -\phi_1 q_1 - \phi_2 q_2, \\ \mathbf{X}_5 &= +\phi_1 q_1 - \phi_2 q_2, \end{aligned} \quad (8)$$

which results in the following set of 3 equations with a_{12} , b_{112} , b_{211} as unknowns:

$$\begin{aligned} \tilde{\mathbf{F}}_{\text{NL}}^{(1)}(\mathbf{X}_3) &= \alpha_{11}^{(1)} q_1^2 + b_{111}^{(1)} q_1^3 + \alpha_{12}^{(1)} q_1 q_2 + \alpha_{22}^{(1)} q_2^2 \\ &\quad + b_{112}^{(1)} q_1^2 q_2 + b_{122}^{(1)} q_1 q_2^2 + b_{222}^{(1)} q_2^3, \\ \tilde{\mathbf{F}}_{\text{NL}}^{(1)}(\mathbf{X}_4) &= \alpha_{11}^{(1)} q_1^2 - b_{111}^{(1)} q_1^3 + \alpha_{12}^{(1)} q_1 q_2 + \alpha_{22}^{(1)} q_2^2 \\ &\quad - b_{112}^{(1)} q_1^2 q_2 - b_{122}^{(1)} q_1 q_2^2 - b_{222}^{(1)} q_2^3, \\ \tilde{\mathbf{F}}_{\text{NL}}^{(1)}(\mathbf{X}_5) &= \alpha_{11}^{(1)} q_1^2 + b_{111}^{(1)} q_1^3 - \alpha_{12}^{(1)} q_1 q_2 + \alpha_{22}^{(1)} q_2^2 \\ &\quad - b_{112}^{(1)} q_1^2 q_2 + b_{122}^{(1)} q_1 q_2^2 - b_{222}^{(1)} q_2^3. \end{aligned} \quad (9)$$

Since all of the uncoupled parameters ($\alpha_{jk}^{(r)}$ and $b_{jkl}^{(r)}$ where $j = k = l$) are already known thanks to the previous step, the coupling terms between two modes ($\alpha_{jkl}^{(r)}$ and $b_{jkl}^{(r)}$ where $j = k \neq l$, etc.) can be found by solving these three linearly independent equations (Eq. (9)). In case of coupling between 3 modes of vibration, the third mode's eigenvector shall also be included in the prescribed displacement, i.e., $\mathbf{X}_c = \phi_j q_j + \phi_k q_k + \phi_l q_l$, and a similar procedure shall be followed to obtain $b_{jkl}^{(r)}$,

where $j \neq k \neq l$. We note that this procedure can be generalized and easily applied to a system with L number of modes.

The number of eigenmodes to consider depends on the complexity of the problem and the dynamic range of interest. In our study, and in order to replicate the nonlinear dynamics observed in Fig. 1b, we used 11 out-of-plane modes in a frequency range that spans 20 MHz to 90 MHz. For convenience, we compare in Tab. I the coupling terms for the first two axisymmetric modes of an ideal (with uniform tension) nanodrum, obtained analytically (see Supplementary Information I) [13] with the FE-based ROM approach explained here. We also provide the quadratic and cubic nonlinear terms of the experimentally tested graphene nanodrum for seven modes of vibration in Tab. 4 of Supplementary Information II. As additional examples, we also provide the nonlinear ROM parameters extracted from this protocol for various other nanomechanical systems such as nanomechanical strings and rectangular membrane resonators in Supplementary Information II.

It is important to mention that the ROM approach sketched here can also account for the influence of in-plane modes of vibration on the nonlinear terms associated with out-of-plane DOFs. This is of great importance for probing nonlinear stiffness terms with accuracy since it has been shown that neglecting the influence of in-plane modes could result in overestimation of the stiffness [16, 25]. In the analytical setting, effects of in-plane modes could be condensed into the out-of-plane modes by assuming zero in-plane inertia since they have orders of magnitude higher frequencies, thus from the frame of reference of out-of-plane modes, act almost instantaneously. In this way they can be treated statically and their effects can be condensed into the out-of-plane modes, without having to calculate their inertial effects [26]. Instead of including the in-plane modes, the FEM method described here can automatically include their effect more efficiently by leaving the in-plane displacements free (instead of fixed) while applying the out-of-plane membrane displacement \mathbf{X}_c . As such, in-plane effects are automatically condensed into the nonlinear parameters out-of-plane modes. After the construction of $\boldsymbol{\eta}$ and the nonlinear ROM, we incorporate the coupled nonlinear differential equations in a numerical continuation package (AUTO) [27] and obtain the steady-state response for different drive frequencies and drive levels, i.e., the frequency response (step V in Fig. 2). We utilize the numerical continuation software also to detect bifurcations in the system, which are crucial for understanding the complex nonlinear dynamics of nanoresonators.

We simulate the ROM for different direct and parametric drive levels, $\tilde{F}^{(r)}(t) = F_{\text{dir}}^{(r)} + F_{\text{par}}^{(r)}$, where $F_{\text{dir}}^{(r)} = J^{(r)} \beta \cos(\omega_d t)$ and $F_{\text{par}}^{(r)} = J^{(r)} q_r \gamma \cos(\omega_d t)$, with γ denoting the parametric drive intensity, β the direct drive

	Analytic		STEP	
	Mode 1	Mode 2	Mode 1	Mode 2
b_{111}	2.84	-0.57	2.84	-0.57
b_{222}	-3.32	22.76	-3.29	22.9
b_{112}	-1.73	9.25	-1.71	9.27
b_{122}	9.25	-9.96	9.27	-9.85

TABLE I: Comparison of the nonlinear coupling coefficients for the first two axisymmetric modes of the graphene nanodrum obtained by an analytical method and the ROM approach. Coefficients are normalized by $c = Eh/r^2$ where E is the Young modulus, h is the thickness and r is the radius of the membrane. We note that the quadratic coupling terms are all zero for a flat symmetric membrane.

intensity, and \mathbf{J} the force mapping vector. We shall note that in order to obtain the modal forces $J^{(r)}$ we use the Duffing shift in the frequency of the high amplitude saddle-node points per drive level. For simplicity, in our simulations we use the Q factor of the fundamental mode ($Q = 180$) for all the modes.

Fig. 3b shows the simulated frequency response of the nonlinear ROM for various drive levels. Simulations are in good qualitative agreement with the experimental frequency responses in both linear and nonlinear regimes. Although it was attempted to obtain quantitative agreement in the nonlinear regime, this was not fully achieved, possibly due to small imperfections in the membrane that deviate its behavior from the FE model. Similar to experiments, it is possible to observe period doubling bifurcations of modes $f_{0,1}$ and $f_{1,1}$ around $\omega_d = 2f_{0,1}$ and $\omega_d = 2f_{1,1}$ caused by the parametric drive. When the first parametric resonance reaches the vicinity of the second asymmetric mode $f_{2,1}$, it suffers a reduction in the simulated responsivity in Fig. 3b which is consistent with the experimental observation in Fig. 1b. We also see the frequency locking at the internal resonance. With further increase in the drive level, similar to the experiments, we observe that the frequency locking “barrier” is broken, and the frequency of parametric resonance peak surges to 3.5 times the frequency of the fundamental mode $f_{0,1}$. After the surge, we also note the presence of the Neimark-Sacker bifurcation nearby the internal resonance at $\omega_d/\omega_0 = 2.538$, which indicates the emergence of aperiodic oscillations [13, 28].

The experiments and simulations depicted in Figs. 1b and 3 demonstrate that, rather than being governed by just two DOFs, the complex motion of the graphene nanodrum around $2.5f_{0,1}$ is a combination of interactions between multiple modes of vibration. We examine the contribution of numerous vibrational modes in the vicinity of the first parametric resonance in order to trace the energy redistribution among various interacting modes. Fig. 4a shows strong activation of multiple modes at the internal resonance point, where axisymmetric modes $f_{0,2}$ and $f_{0,3}$ (mode numbers 6 and 15) with asymmetric mode $f_{2,1}$ (mode number 4) are most notably excited. Time re-

sponses of the modes during one period of $f_{0,1}$ oscillation at $\omega_d/\omega_0 = 2.538$ are also shown for convenience (Supplementary Information III). A more visual representation of the time signals can be obtained by using the modal amplitudes q from AUTO to superpose the FEM mode shapes ϕ , thereby reconstructing the total mechanical response and the deflection shape \mathbf{X} of the graphene nanodrum during internal resonance (see Fig. 4b and 4c). If we analyze the nanodrum shape at its maximum amplitude level during an oscillation, we can see that the effective deflection shape is unique near the internal resonance point (Fig. 4b). Dissecting the total motion of the membrane by taking snapshots at different times during a single period of the fundamental mode $f_{0,1}$ (Fig. 4c) further reveals the strong influence of the multi-modal interaction. It is possible to clearly observe the emergence of other mode shapes during a single oscillation of $f_{0,1}$ parametric resonance. These simulations clearly showcase the energy pathways that lead to the aforementioned nonlinear dissipation phenomenon, not only at the clearly visible internal resonance, but also at responses that look regular, like the direct resonance of $f_{0,1}$. When the global frequency response per mode is analyzed, it is also possible to see the autoparametric activation of multiple modes around the $f_{0,1}$ where most of the energy ends up in $f_{0,3}$ (see Supplementary Information III).

We note that the favored energy pathways for each system will be distinct due to variations in pre-tension, geometry, and material properties. These physical parameters dictate the system’s capacity to “internally resonate”, due to their effects on the nonlinear terms and resonance frequencies. In the literature, it is common to model nonlinear systems by disregarding the effects of multi-modal interactions, especially if there are no other visible modes contributing to the measurement data. Most of the time, as discussed before, this results in using empirical fit parameters to explain the observations. In this case, the assumption is that, all the interactions effectively renormalize the terms in the single mode equation (generally being Duffing or Duffing-van der Pol). The downfall of this assumption is that, in reality, the effects of multi-modal interactions are amplitude and drive frequency dependent [9], whereas renormalization through empirical fit parameters assumes constant effects. This means that such simplistic models, at best, will agree with the experiments only for a snapshot of frequency response and cannot explain the overall dynamics at higher drive levels and for wide frequency ranges. Utilizing a method that fully relies on physical parameters and includes as many modes as needed, automatically resolves this problem, while clearly displaying the enigmatic nature of these intermodal interactions and energy dissipation pathways.

In summary, we utilized a nonlinear ROM technique to characterize the multi-modal interactions of nanomechanical resonators. We used FEM simulations as the

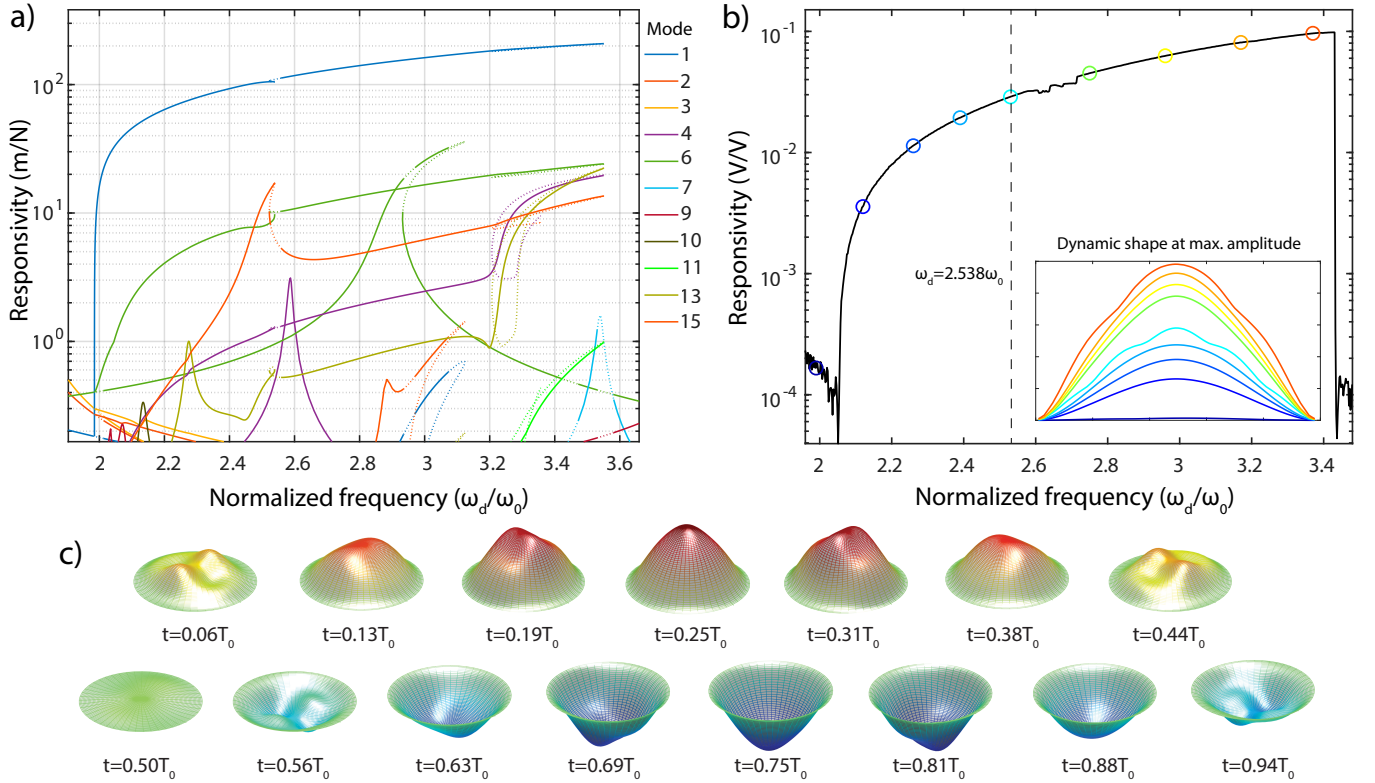


FIG. 4: Simulated overall nonlinear dynamic response of the graphene membrane at principal parametric resonance of $f_{0,1}$. a) Simulated shape of the membrane at maximum amplitude level during its parametric resonance at specific drive frequencies, displayed on the experimental parametric resonance curve. Solid lines indicate stable solutions whereas dashed lines indicate unstable ones. b) Full simulated frequency response at the principal parametric resonance of mode $f_{0,1}$, showing activation of many other modes in the system during the strong parametric resonance, specially around the internal resonance region $\omega_d/\omega_0 = 2.538$. c) Shape of the membrane during a period of oscillation at internal resonance ($\omega_d/\omega_0 = 2.538$), displaying multiple mode shapes within a single period of oscillation with different frequencies. T_0 is a single period of mode $f_{0,1}$. Amplitude of the response is amplified for visual convenience.

basis to develop our physics-based model, that relies purely on measurable quantities from experiments. We calculated the linear and nonlinear internal forces using FEM simulations to extract quadratic and cubic nonlinear terms for constructing the full nonlinear ROM. By simulating the response curves with the model and comparing the results to nonlinear dynamic measurements of a graphene nanodrum resonator, we showed that the model can replicate complex nonlinear intermodal interactions. Moreover, by tracking simultaneous activation of modal amplitudes, we have identified intermodal energy transfer pathways mediated by nonlinear couplings between multiple modes of vibration. Our study provides an efficient and accurate protocol for modelling complex nonlinear dynamics of nanomechanical resonators in a global manner, purely based on material and geometrical parameters. As a result, we anticipate that this protocol will not only aid in explaining the multi-mode nonlinear dynamics of nanoresonators, but will also serve as a framework for designing optimized nanoresonators that can take advantage of the powerful phenomena that non-

linear dynamics has to offer [29, 30].

-
- [1] J. Chaste, A. Eichler, J. Moser, G. Ceballos, R. Rurali, and A. Bachtold, “A nanomechanical mass sensor with yoctogram resolution,” *Nature Nanotechnology*, vol. 7, pp. 301–304, May 2012.
 - [2] F. Fogliano, B. Besga, A. Reigue, L. Mercier de Lépinay, P. Heringlake, C. Gouriou, E. Eyraud, W. Wernsdorfer, B. Pigeau, and O. Arcizet, “Ultrasensitive nano-optomechanical force sensor operated at dilution temperatures,” *Nature Communications*, vol. 12, p. 4124, Jul 2021.
 - [3] I. E. Rosloń, A. Japaridze, P. G. Steeneken, C. Dekker, and F. Alijani, “Probing nanomotion of single bacteria with graphene drums,” *Nature Nanotechnology*, vol. 17, no. 6, pp. 637–642, 2022.
 - [4] A. Bachtold, J. Moser, and M. Dykman, “Mesoscopic physics of nanomechanical systems,” *Reviews of Modern Physics*, vol. 94, no. 4, p. 045005, 2022.

- [5] P. G. Steeneken, R. J. Dolleman, D. Davidovikj, F. Alijani, and H. S. J. van der Zant, “Dynamics of 2d material membranes,” *2D Materials*, vol. 8, p. 042001, Aug 2021.
- [6] R. Lifshitz and M. C. Cross, *Nonlinear Dynamics of Nanomechanical and Micromechanical Resonators*, ch. 1, pp. 1–52. John Wiley & Sons, Ltd, 2008.
- [7] A. H. Nayfeh and D. T. Mook, *Nonlinear Oscillations*, vol. 57 of *Wiley Classics Library*. Wiley-VCH, Mar 1995.
- [8] J. Güttinger, A. Noury, P. Weber, A. M. Eriksson, C. Lagoin, J. Moser, C. Eichler, A. Wallraff, A. Isacsson, and A. Bachtold, “Energy-dependent path of dissipation in nanomechanical resonators,” *Nature Nanotechnology*, vol. 12, pp. 631–636, jul 2017.
- [9] A. Keşkekler, O. Shoshani, M. Lee, H. S. J. van der Zant, P. G. Steeneken, and F. Alijani, “Tuning nonlinear damping in graphene nanoresonators by parametric–direct internal resonance,” *Nature Communications*, vol. 12, p. 1099, Feb 2021.
- [10] D. Antonio, D. H. Zanette, and D. López, “Frequency stabilization in nonlinear micromechanical oscillators,” *Nature communications*, vol. 3, no. 1, pp. 1–6, 2012.
- [11] M. Wang, D. J. Perez-Morelo, D. Lopez, and V. A. Aksyuk, “Persistent nonlinear phase-locking and non-monotonic energy dissipation in micromechanical resonators,” *Phys. Rev. X*, vol. 12, p. 041025, Dec 2022.
- [12] C. Chen, D. H. Zanette, D. A. Czaplewski, S. Shaw, and D. López, “Direct observation of coherent energy transfer in nonlinear micromechanical oscillators,” *Nature Communications*, vol. 8, p. 15523, May 2017.
- [13] A. Keşkekler, H. Arjmandi-Tash, P. G. Steeneken, and F. Alijani, “Symmetry-breaking-induced frequency combs in graphene resonators,” *Nano Letters*, vol. 22, pp. 6048–6054, Aug 2022.
- [14] D. A. Czaplewski, C. Chen, D. Lopez, O. Shoshani, A. M. Eriksson, S. Strachan, and S. W. Shaw, “Bifurcation generated mechanical frequency comb,” *Phys. Rev. Lett.*, vol. 121, p. 244302, Dec 2018.
- [15] J. S. Ochs, G. Rastelli, M. Seitner, M. I. Dykman, and E. M. Weig, “Resonant nonlinear response of a nanomechanical system with broken symmetry,” *Phys. Rev. B*, vol. 104, p. 155434, Oct 2021.
- [16] D. Davidovikj, F. Alijani, S. J. Cartamil-Bueno, H. S. J. van der Zant, M. Amabili, and P. G. Steeneken, “Nonlinear dynamic characterization of two-dimensional materials,” *Nat Commun*, vol. 8, p. 1253, 2017.
- [17] D. Midtvedt, A. Croy, A. Isacsson, Z. Qi, and H. S. Park, “Fermi-pasta-ulam physics with nanomechanical graphene resonators: Intrinsic relaxation and thermalization from flexural mode coupling,” *Phys. Rev. Lett.*, vol. 112, p. 145503, Apr 2014.
- [18] B. Sajadi, S. Wahls, S. van Hemert, P. Belardinelli, P. G. Steeneken, and F. Alijani, “Nonlinear dynamic identification of graphene’s elastic modulus via reduced order modeling of atomistic simulations,” *Journal of the Mechanics and Physics of Solids*, vol. 122, pp. 161–176, 2019.
- [19] R. J. Dolleman, S. Houry, A. Chandrashekar, F. Alijani, H. S. Van Der Zant, and P. G. Steeneken, “Optothermally excited multimode parametric resonance in graphene membranes,” *Scientific reports*, vol. 8, no. 1, pp. 1–7, 2018.
- [20] A. Eichler, J. Moser, J. Chaste, M. Zdrojek, I. Wilson-Rae, and A. Bachtold, “Nonlinear damping in mechanical resonators made from carbon nanotubes and graphene,” *Nature Nanotechnology*, vol. 6, pp. 339–342, Jun 2011.
- [21] A. A. Muravyov and S. A. Rizzi, “Determination of nonlinear stiffness with application to random vibration of geometrically nonlinear structures,” *Computers & Structures*, vol. 81, no. 15, pp. 1513 – 1523, 2003.
- [22] B. Sajadi, S. van Hemert, B. Arash, P. Belardinelli, P. G. Steeneken, and F. Alijani, “Size- and temperature-dependent bending rigidity of graphene using modal analysis,” *Carbon*, vol. 139, pp. 334–341, 2018.
- [23] A. Castellanos-Gomez, V. Singh, H. S. J. van der Zant, and G. A. Steele, “Mechanics of freely-suspended ultrathin layered materials,” *Annalen der Physik*, vol. 527, no. 1-2, pp. 27–44, 2015.
- [24] A. Isacsson, A. W. Cummings, L. Colombo, L. Colombo, J. M. Kinaret, and S. Roche, “Scaling properties of polycrystalline graphene: a review,” *2D Materials*, vol. 4, p. 012002, dec 2016.
- [25] A. Sarafraz, A. Givois, I. Roslon, H. Liu, H. Brahmī, G. Verbiest, P. G. Steeneken, and F. Alijani, “Dynamics of pressurized ultra-thin membranes,” *arXiv.org*, Dec 2022.
- [26] M. P. Mignolet, A. Przekop, S. A. Rizzi, and S. M. Spottswood, “A review of indirect/non-intrusive reduced order modeling of nonlinear geometric structures,” *Journal of Sound and Vibration*, vol. 332, no. 10, pp. 2437–2460, 2013.
- [27] E. J. Doedel, A. R. Champneys, F. Dercole, T. F. Fairgrieve, Y. A. Kuznetsov, B. Oldeman, R. Paffenroth, B. Sandstede, X. Wang, and C. Zhang, “Auto-07p: Continuation and bifurcation software for ordinary differential equations,” 2007.
- [28] G. Gobat, V. Zega, P. Fedeli, C. Touzé, and A. Frangi, “Frequency combs in a mems resonator featuring 1:2 internal resonance: ab initio reduced order modelling and experimental validation,” *Nonlinear Dynamics*, vol. 111, pp. 2991–3017, Feb 2023.
- [29] S. Dou, B. S. Strachan, S. W. Shaw, and J. S. Jensen, “Structural optimization for nonlinear dynamic response,” *Philosophical Transactions of the Royal Society A: Mathematical, Physical and Engineering Sciences*, vol. 373, no. 2051, p. 20140408, 2015.
- [30] L. L. Li, P. M. Polunin, S. Dou, O. Shoshani, B. Scott Strachan, J. S. Jensen, S. W. Shaw, and K. L. Turner, “Tailoring the nonlinear response of mems resonators using shape optimization,” *Applied Physics Letters*, vol. 110, no. 8, p. 081902, 2017.

Supplementary Information

Characterizing multi-mode nonlinear dynamics of nanomechanical resonators

Ata Keşkekler^{*1}, Vincent Bos¹, Alejandro M. Aragón¹, Peter G. Steeneken^{1,2}, and
Farbod Alijani^{*1}

¹Department of Precision and Microsystems Engineering, TU Delft, The Netherlands

²Kavli Institute of Nanoscience, TU Delft, The Netherlands

April 3, 2023

Contents

1	Analytical model for ideal membrane with two-degrees-of-freedom	2
2	Nonlinear reduced-order model parameters for different nanomechanical resonators	3
2.1	Reduced-order model parameters for the experimental graphene drum	3
2.2	Reduced-order model parameters for a square membrane resonator	7
2.3	Reduced-order model parameters for a string resonator	10
3	Dynamic response of the graphene drum during internal resonance	12

*Corresponding authors:

Ata Keşkekler <a.keskekler-1@tudelft.nl>,
Farbod Alijani <f.alijani@tudelft.nl>

1 Analytical model for ideal membrane with two-degrees-of-freedom

In order to benchmark the method provided in the main text, we use the Rayleigh-Ritz approach to obtain the equations of motion for a circular membrane [1, 2, 3]. The elastic strain energy of the drum is obtained as

$$U = \int_0^{2\pi} \int_0^R \frac{Eh}{2(1-\nu^2)} \left(\epsilon_{rr}^2 + \epsilon_{\theta\theta}^2 + 2\nu\epsilon_{rr}\epsilon_{\theta\theta} + \frac{1-\nu}{2}\gamma_{r\theta}^2 \right) r dr d\theta, \quad (1)$$

in which h is the thickness of the drum, R is the radius, E is the Young's modulus, and ν is the Poisson's ratio. Moreover, ϵ_{rr} , $\epsilon_{\theta\theta}$, and $\gamma_{r\theta}$ are the normal and shear strains. During axisymmetric oscillations $\gamma_{r\theta} = 0$, and the normal strains are obtained in terms of the transverse deflection (w) and radial displacement (u) of the drum as follows

$$\epsilon_{rr} = \frac{\partial u}{\partial r} + \frac{1}{2} \left(\frac{\partial w}{\partial r} \right)^2 + \left(\frac{\partial w}{\partial r} \right) \left(\frac{\partial w_0}{\partial r} \right), \quad (2)$$

$$\epsilon_{\theta\theta} = \frac{u}{r}. \quad (3)$$

In Eq.(2), w_0 is the initial transverse displacement of the drum associated with zero initial stress, and is equal to zero when assuming ideal symmetric membrane. By taking into account the modal interactions between the first two axisymmetric eigenmodes and fixed boundary conditions ($u = w = 0$), the solution is approximated as

$$w = q_1(t)J_0\left(Z_1 \frac{r}{R}\right) + q_2(t)J_0\left(Z_2 \frac{r}{R}\right), \quad (4)$$

$$u = u_0 r + r(R-r) \sum_{j=1}^n y_j(t)r^{j-1}, \quad (5)$$

where u_0 is the initial radial displacement due to pre-tension n_0 , and q_1 and q_2 are generalized coordinates associated with the first and the second axisymmetric mode of the drum, respectively. Moreover, J_0 is the Bessel function of order zero and Z_1 and Z_2 are its first two roots. We Taylor approximate $J_0\left(Z_1 \frac{r}{R}\right)$ to 10th order and $J_0\left(Z_2 \frac{r}{R}\right)$ to 14th order to accurately capture the mode shapes. In addition, y_j are the radial generalized coordinates and n is the number of these coordinates retained in the approximation where convergence is achieved at $n = 8$.

The kinetic energy of the drum is then obtained as

$$T = \frac{1}{2}\rho h \int_0^{2\pi} \int_0^R \dot{w}^2 r dr d\theta, \quad (6)$$

in which the overdot represents differentiation with respect to time t , and ρ is the mass density.

Next, we obtain Lagrange equations as follows:

$$\frac{\partial \mathcal{L}}{\partial q_i} - \frac{d}{dt} \left(\frac{\partial \mathcal{L}}{\partial \dot{q}_i} \right) = 0, \quad (7)$$

where \mathcal{L} is the Lagrangian ($\mathcal{L} = T - U$), resulting in the equations:

$$m_1 \ddot{q}_1 + k_1 q_1 + \alpha_{11}^{(1)} q_1^2 + \alpha_{12}^{(1)} q_1 q_2 + \alpha_{22}^{(1)} q_2^2 + b_{111}^{(1)} q_1^3 + b_{112}^{(1)} q_1^2 q_2 + b_{122}^{(1)} q_1 q_2^2 + b_{222}^{(1)} q_2^3 = 0, \quad (8)$$

$$m_2 \ddot{q}_2 + k_2 q_2 + \alpha_{11}^{(2)} q_1^2 + \alpha_{12}^{(2)} q_1 q_2 + \alpha_{22}^{(2)} q_2^2 + b_{111}^{(2)} q_1^3 + b_{112}^{(2)} q_1^2 q_2 + b_{122}^{(2)} q_1 q_2^2 + b_{222}^{(2)} q_2^3 = 0, \quad (9)$$

in which $\alpha_{jk}^{(r)}$ and $b_{jkl}^{(r)}$ are the quadratic and cubic nonlinear terms. It is possible to express the coefficients in the equations of motion in terms of mechanical and geometric properties of the drum as follows

$$\omega_1 = \sqrt{\frac{k_1}{m_1}} = \frac{2.4}{R} \sqrt{\frac{n_0}{\rho h}} \quad (10a)$$

$$\omega_2 = \sqrt{\frac{k_2}{m_2}} = \frac{5.5}{R} \sqrt{\frac{n_0}{\rho h}}, \quad (10b)$$

$$b_{111}^{(1)} = 2.84 \frac{Eh}{R^2}, b_{111}^{(2)} = -0.57 \frac{Eh}{R^2} \quad (10c)$$

$$b_{222}^{(1)} = -3.32 \frac{Eh}{R^2}, b_{222}^{(2)} = 22.76 \frac{Eh}{R^2} \quad (10d)$$

$$b_{112}^{(1)} = -1.73 \frac{Eh}{R^2}, b_{112}^{(2)} = 9.25 \frac{Eh}{R^2} \quad (10e)$$

$$b_{122}^{(1)} = 9.25 \frac{Eh}{R^2}, b_{122}^{(2)} = -9.96 \frac{Eh}{R^2} \quad (10f)$$

in which the coefficients were evaluated assuming $\nu = 0.16$. The quadratic terms $\alpha_{jk}^{(r)}$ are all zero due to the ideal symmetric membrane assumption ($w_0 = 0$).

2 Nonlinear reduced-order model parameters for different nanomechanical resonators

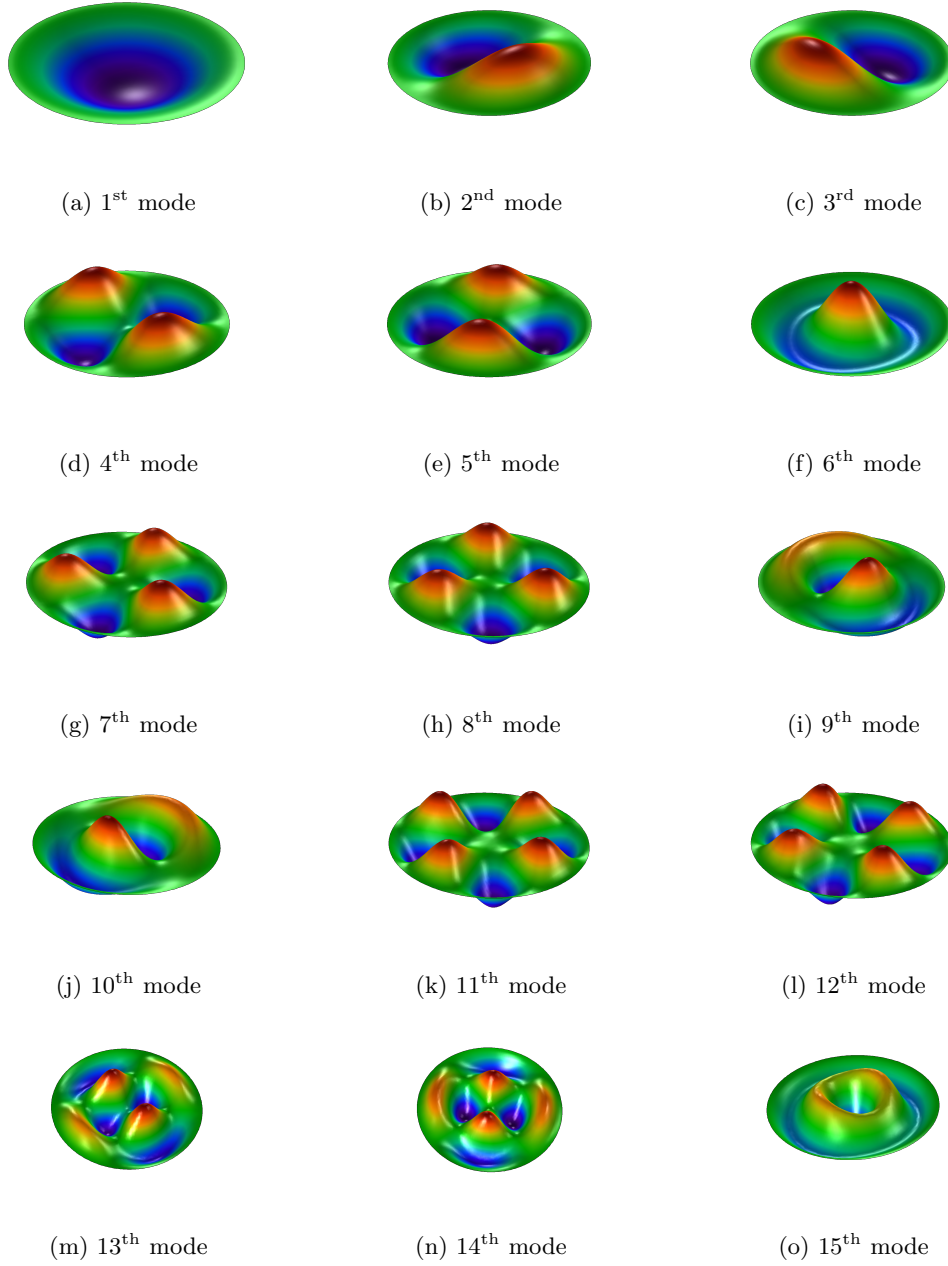
Here we provide the nonlinear reduced-order model parameters extracted using the STEP method [4], for the graphene nanodrum discussed in the main text, as well as a rectangular membrane and a string resonator. In the following tables, it is possible to find the definitions of the physical parameters for each model, dimensional prefactors for the terms in the nonlinear reduced-order model, and the dimensionless coefficients for the nonlinear terms. We note that for flat ideal circular, square and string resonators, the quadratic nonlinear terms are nonexistent for out-of-plane modes in the absence of in-plane modes.

2.1 Reduced-order model parameters for the experimental graphene drum

Reduced-order model of the graphene drum is based on a finite element (FE) model constructed in COMSOL, considering fixed boundary condition with plate elements. Eigenmodes of the graphene drum can be found in Supplementary Fig. 1. The description of model parameters, scaling values and linear modal parameters can be found in Supplementary Tables 1, 2 and 3. We construct the model using the first three axisymmetric and first four asymmetric out-of-plane modes of the structure, excluding their degenerates. Nonlinear coefficients can be found in Supplementary Table 4.

Supplementary Table 1: Parameters for the graphene drum resonator

Parameter	Formula	Units	Description
E	-	Pa	Young's modulus
h	-	m	Thickness
R	-	m	Radius
ν	-	-	Poisson's ratio
ρ	-	kg/m ³	Density
σ	-	Pa	Stress
$\tilde{\rho}$	ρh	kg/m ²	Mass per unit area
T_0	σh	N m ⁻¹	Membrane tension



Supplementary Figure 1: Eigenmodes of the graphene drum resonator

Supplementary Table 2: Scaling values for the graphene drum equations

m_t	Linear		Nonlinear	
	k_0	ω_0	a_{dim}	b_{dim}
$\pi R^2 h \rho$	T_0	$\frac{2.405}{R} \sqrt{\frac{T_0}{\bar{\rho}}}$	$[-]$	$\frac{Eh}{R^2}$

Supplementary Table 3: Dimensionless linear modal values for the experimental graphene drum from the main text. Eigenfrequencies are normalized w.r.t. the fundamental mode (ω_1). Modes: 1,2,4,6,7,9,15

	Eq. 1	Eq. 2	Eq. 3	Eq. 4	Eq. 5	Eq. 6	Eq. 7
m/m_t	0.204	0.195	0.183	0.103	0.192	0.118	0.0698
k/k_0	5.78	16.5	34.6	24.2	68.3	55.4	64.9
ω/ω_1	1	1.73	2.59	2.89	3.54	4.07	5.73

Supplementary Table 4: Dimensionless nonlinear coefficients for the graphene drum ($\nu = 0.16$) from the main text. Modes: 1,2,4,6,7,9,15.

	Eq. 1	Eq. 2	Eq. 3	Eq. 4	Eq. 5	Eq. 6	Eq. 7
b_{111}	2.55	0	0.313	1.34	0.000 204	0.000 435	-0.529
b_{112}	0	8.57	-0.000 307	-0.000 596	-0.426	-4.05	0.000 196
b_{113}	0.942	-0.000 283	9.79	1.07	-0.001 11	0.000 244	-0.0467
b_{114}	4.02	-0.000 585	1.07	10.8	0.001 24	-0.000 745	2.96
b_{115}	0.000 58	-0.434	-0.001 09	0.001 24	12	0.71	0.000 527
b_{116}	0.001 28	-4.05	0.000 289	-0.000 762	0.711	15.9	0.0028
b_{117}	-1.61	0.000 168	-0.0469	2.96	0.000 479	0.0028	14.2
b_{122}	8.61	0	-5.82	3.82	0.001 54	0.002 08	-2.56
b_{123}	-0.143	-11.8	0.349	0.0771	-13.8	7.28	0.0707
b_{124}	0.001 29	7.69	0.0838	0.167	0.621	-14.5	0.08
b_{125}	-0.826	0.174	-13.7	0.625	0.434	0.0744	2.17
b_{126}	-8.12	0.0522	7.31	-14.5	0.0669	0.26	0.184
b_{127}	-0.0667	-5.07	0.0861	0.0629	2.17	0.158	0.361
b_{133}	9.88	0.000 849	1.46	1.37	-0.000 543	0.002 17	-7.65
b_{134}	2.13	0.000 409	2.83	6.92	0.002 48	-0.000 509	4.82
b_{135}	-0.0277	-13.7	0.22	-0.000 755	1.95	6.94	-0.0145
b_{136}	-0.001 52	7.33	0.085	0.019	6.94	-9.79	-0.006 23
b_{137}	-0.0863	-0.000 881	-15.3	4.82	0.0112	-0.003 04	10.5
b_{144}	10.8	-0.000 906	3.54	17.4	0.001 68	-0.000 612	8.08
b_{145}	0.0254	0.634	0.0135	0.133	-1.84	2.25	-0.0204
b_{146}	0.0829	-14.4	0.0383	0.167	2.25	34	-0.006 71
b_{147}	5.92	-0.005 01	4.86	16.3	0.003 22	0.0132	28.8
b_{155}	12.1	-0.000 487	1.18	-1.01	-0.001 61	0.005 79	-11.1
b_{156}	1.45	0.02	7.02	2.27	0.197	0.293	-0.336
b_{157}	-0.032	2.16	-0.000 708	-0.0264	-22.1	-0.336	0.136
b_{166}	16.1	0.002 54	-4.79	16.8	0.006 14	-0.0112	2.66
b_{167}	-0.033	0.161	-0.001 44	-0.0053	-0.335	5.38	0.144
b_{177}	14.4	-0.006 84	5.31	14.3	0.002 16	0.0112	3.13
b_{222}	0	18.7	-0.000 908	-0.001 43	1.94	-6.99	0.000 362
b_{223}	-5.73	-0.002 72	45.2	6.43	-0.004 45	-0.001 77	6.38
b_{224}	3.83	-0.004 33	6.42	16	0.001 59	-0.001 27	3.57
b_{225}	0.001 46	5.81	-0.004 34	0.001 56	47.7	4.2	-0.009 25
b_{226}	0.001 94	-21	-0.001 57	-0.001 27	4.21	53	0.0126
b_{227}	-2.48	0.000 901	6.38	3.55	-0.009 39	0.0125	22.2
b_{233}	0.000 75	45.2	-0.004 85	-0.004 84	31.9	-5.51	-0.004 98
b_{234}	0.004 52	12.9	-0.005 23	-0.0825	20.3	7.73	-0.0346
b_{235}	-13.5	-0.224	64	20.3	-0.399	-0.0729	15.6
b_{236}	7.3	0.0157	-10.9	7.74	-0.0876	-0.285	-9.19
b_{237}	-0.0112	12.8	-0.0207	-0.0566	15.6	-9.18	-0.158
b_{244}	-0.000 933	16	-0.002 87	-0.003 74	-3.94	-14.1	-0.007 15
b_{245}	0.605	0.008 98	20.3	-7.81	0.0907	0.002 22	-2.75
b_{246}	-14.3	-0.0382	7.73	-28.1	0.002 47	0.15	-11.7
b_{247}	0.0374	7.29	0.0448	0.237	-2.76	-11.8	0.376
b_{255}	-0.000 489	47.8	0.004 69	-0.001 45	0.0154	10.7	-0.012
b_{256}	-0.004 83	8.51	-0.004 51	-0.0111	21.5	5.05	0.000 509
b_{257}	2.13	-0.0207	15.6	-2.74	0.007 64	0.006 18	-12.7
b_{266}	0.002 43	53.3	-0.0148	0.004 74	2.42	-66.2	-0.018
b_{267}	-0.108	-0.0164	-9.17	-11.7	0.0066	0.0415	-29.3
b_{277}	-0.006 64	22.3	-0.004 88	-0.0109	-6.38	-14.7	-0.005 34
b_{333}	0.476	-0.001 44	44.9	4.06	-0.005 68	-0.001 14	0.176
b_{334}	1.35	-0.004 73	12.2	45.4	-0.000 223	-0.0106	8.8
b_{335}	-0.000 782	31.8	-0.0168	-0.000 288	121	11.2	-0.006 72
b_{336}	0.002 11	-5.46	-0.002 99	-0.0106	11.2	54.8	-0.008 19
b_{337}	-7.59	-0.005 04	0.53	8.78	-0.007 05	-0.008 23	45.1
b_{344}	3.5	-0.002 79	45.4	0.37	-0.005 26	-0.003 48	5.32
b_{345}	-0.005 34	20.2	0.0276	-0.0768	5.01	58.3	-0.0532
b_{346}	-0.007 06	7.68	-0.006 18	-0.0376	58.3	12.7	0.002 49
b_{347}	4.81	-0.000 293	17.6	10.5	-0.0412	0.0192	4.01
b_{355}	1.15	0.004 91	121	2.55	0.000 372	-0.002	-6.49
b_{356}	6.9	-0.0452	22.4	58.3	-0.145	-0.213	-14
b_{357}	-0.000 73	15.5	0.003 02	-0.0546	-13	-14	-0.085
b_{366}	-4.85	-0.0145	54.9	6.4	-0.0298	0.009 73	11.9
b_{367}	-0.005 78	-9.12	-0.003 29	0.001 84	-14	23.8	-0.0382
b_{377}	5.24	-0.004 72	45.1	2.09	-0.003 47	0.0116	-2.47
b_{444}	5.72	-0.001 18	0.121	26.5	0.001 94	-0.001 52	13.7
b_{445}	0.001 57	-3.92	-0.005 16	0.005 24	57.3	-4.5	0.0103
b_{446}	-0.000 414	-14	-0.003 38	-0.005 93	-4.5	61.5	0.0181
b_{447}	8.05	-0.007 03	5.31	41.1	0.0101	0.0182	70.8
b_{455}	-1.05	-0.001 39	2.54	57.3	0.004 56	-0.003 35	-11.8
b_{456}	2.22	-0.007 29	58.3	-8.97	0.0408	0.0648	8.01
b_{457}	0.0154	-2.73	-0.0417	0.0565	-23.6	8.01	0.0482
b_{466}	16.5	0.005 02	6.39	61.5	-0.007 38	-0.0574	24.7
b_{467}	0.0212	-11.6	0.0228	0.0718	8.01	49.5	0.129
b_{477}	14.1	-0.0106	2.08	70.8	-0.006 54	0.0288	77.4
b_{555}	-0.000 543	0.0125	0.000 385	0.001 93	116	2.28	-0.006 66
b_{556}	0.005 66	10.7	-0.001 35	-0.003 52	6.83	105	-0.0293
b_{557}	-10.9	-0.012	-6.49	-11.8	-0.0234	-0.0292	61.7
b_{566}	0.006 17	2.45	-0.0296	-0.007 28	105	42.2	-0.017
b_{567}	-0.308	-0.001 15	-14	8.01	-0.0505	-0.0185	-4.96
b_{577}	0.001 92	-6.34	-0.003 34	-0.006 72	61.8	-2.49	0.0524
b_{666}	-0.002 65	-21.9	0.0039	-0.0176	14.1	99.4	0.0251
b_{667}	2.89	-0.0179	11.9	24.7	-0.0172	0.077	67.3
b_{677}	0.0108	-14.5	0.0118	0.0285	-2.49	67.3	0.0274
b_{777}	1.13	-0.000 123	-0.814	25.8	0.0211	0.006 82	81.4

2.2 Reduced-order model parameters for a square membrane resonator

Reduced-order model of an ideal square membrane is based on an FE model constructed in COMSOL, considering pinned boundary conditions with membrane elements. Eigenmodes of the square drum can be found in Supplementary Fig. 2. The description of model parameters, scaling values and linear modal parameters can be found in Supplementary Tables 5, 6 and 7. We construct the model using the first eleven out-of-plane modes of the structure, excluding their degenerates, resulting in seven modes. Nonlinear coefficients can be found in Supplementary Table 8.

Supplementary Table 5: Parameters for a square membrane and string resonators

Parameter	Formula	Units	Description
E	-	Pa	Young's modulus
h	-	m	Thickness
L	-	m	Length
ν	-	-	Poisson's ratio
ρ	-	kg/m ³	Density
σ	-	Pa	Stress
$\tilde{\rho}$	ρh	kg/m ²	Mass per unit area
T_0	σh	N m ⁻¹	Membrane tension

Supplementary Table 6: Scaling values for a square membrane resonator

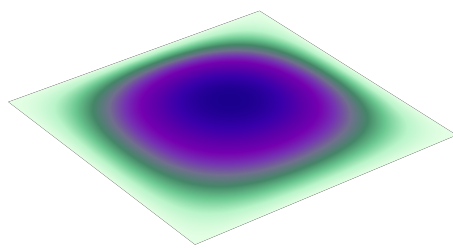
m_t	Linear		a_{dim}	Nonlinear	
	k_0	ω_0		b_{dim}	
$L^2 h \rho$	T_0	$\frac{\pi}{L} \sqrt{\frac{2T_0}{\tilde{\rho}}}$	$[-]$	$\frac{\pi}{1.27 - 0.97\nu} \frac{Eh}{L^2}$	

Supplementary Table 7: Dimensionless linear modal values of a square membrane resonator for modes: 1,2,4,5,7,9,11.

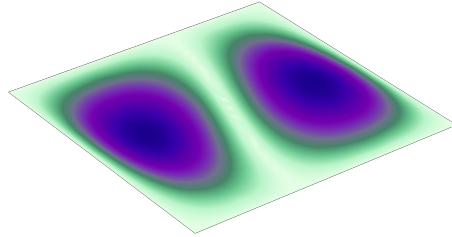
	Eq. 1	Eq. 2	Eq. 3	Eq. 4	Eq. 5	Eq. 6	Eq. 7
m/m_t	0.25	0.215	0.25	0.206	0.154	0.227	0.248
k/k_0	4.93	10.6	19.7	20.3	19.8	38.2	44.2
ω/ω_0	1	1.58	2	2.24	2.55	2.92	3

Supplementary Table 8: Dimensionless nonlinear coefficients for a square membrane resonator modelled with modes: 1,2,4,5,7,9,11.

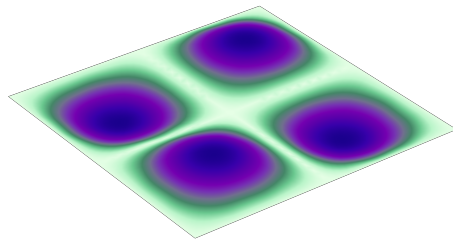
	Eq. 1	Eq. 2	Eq. 3	Eq. 4	Eq. 5	Eq. 6	Eq. 7
b111	3.65	0	0	-0.0807	0	-0.000 131	-0.0466
b112	0	11.6	0	-0.000 267	1.17	-1.17	-0.000 234
b113	0	0	15.2	-0.000 269	0	0	-0.001 12
b114	-0.242	0	-0.000 418	16.4	-0.000 231	-0.000 154	-0.635
b115	0	1.15	0.000 103	-0.000 291	12.9	-1.27	0.001 07
b116	0	-1.13	-0.000 234	-0.000 123	-1.27	31.8	0.002 11
b117	-0.144	-0.000 263	-0.001 17	-0.634	0.000 812	0.001 59	27.4
b122	11.6	-0.000 387	10.4	2.87	-0.000 952	-0.001 5	0.367
b123	-0.0597	20.7	-0.303	-0.0311	-13.7	-8.35	-0.109
b124	-0.0514	5.63	-0.0362	-0.385	4.47	7.54	0.179
b125	2.29	-0.057	-14.1	4.49	-0.193	-0.0697	-18
b126	-2.32	-0.126	-8.16	8	-0.0441	-0.494	-9.19
b127	0.0561	0.791	0.0117	0.0806	-18.2	-8.97	-0.397
b133	15.2	-0.000 448	0.002 01	1.2	0.001 78	-0.003 27	8.13
b134	-0.019	0.001 78	2.29	-0.186	0.000 313	0.006 95	-0.0058
b135	-0.0147	-14	-0.121	-0.005 15	10.3	-9.72	-0.16
b136	-0.0233	-8.18	-0.14	-0.0121	-9.85	-3.8	-0.0321
b137	0.0116	0.001 07	16.5	-0.007 81	0.007 65	-0.006 99	-0.232
b144	16.4	0	0	2.26	-0.001 41	0.004 65	-19.8
b145	-0.0133	4.48	0.003 81	-0.175	3.1	-8.76	0.0714
b146	-0.0633	8.01	0.005 51	-0.26	-8.47	19.2	0.227
b147	-1.16	0.002 15	-0.005 16	-39.3	-0.000 571	0.0115	-0.279
b147	12.9	-0.003 23	5.31	1.64	-0.001 01	-0.001 47	2.64
b155	-2.53	-0.0488	-9.79	-8.34	-0.148	-0.267	-17.9
b156	0.0263	-18.2	-0.0387	0.0259	5.39	-17.6	-0.312
b166	31.8	0.0107	-1.71	9.94	0.0026	-0.0312	0.307
b167	0.061	-9.15	0.000 304	0.189	-17.8	1	-0.458
b177	27.4	0	0.0117	0.2	0.0051	-0.0057	0.11
b222	-0.000 165	21.9	0	0.000 103	-0.117	-1.95	0.000 453
b223	10.5	0.000 308	58.2	2.24	0.002 78	0.0003	8.15
b224	2.91	0	2.24	58.7	-0.003 07	0.005 54	-6.02
b225	-0.000 944	-0.34	0.002 68	-0.002 86	51	-6.71	0.007 85
b226	-0.001 46	-5.86	-0.000 207	0.004 51	-6.71	79.3	-0.000 829
b227	0.307	0.001 35	8.17	-6.03	0.007 68	-0.001 78	69.9
b233	-0.000 749	58.2	-0.002 5	-0.001 13	-28.8	-2.03	-0.0032
b234	-0.0416	4.4	-0.115	-0.19	-7.88	37.6	0.0978
b235	-14.1	0.0428	-57.7	-7.9	-0.224	0.0697	-64.9
b236	-8.21	-0.0898	-4.19	37.7	0.144	-0.495	11.6
b237	-0.008 33	16.4	-0.0144	0.0216	-64.9	11.6	-0.316
b244	0	58.7	0.003 45	0.002 42	34.5	21.1	0.001 02
b245	4.56	-0.0935	-7.91	68.8	-0.267	-0.195	-26.9
b246	8.12	-0.169	37.7	42	-0.116	-0.904	-58.8
b247	0.0902	-12	0.0513	0.398	-26.9	-58.7	-0.63
b255	-0.003 67	51	-0.008 05	-0.006 74	-20.2	10.4	-0.0024
b256	-0.000 602	-13.5	0.0222	-0.0165	20.7	46	0.0198
b257	-18.3	0.0616	-65	-26.9	0.146	0.128	-15.4
b266	0.0114	79.4	0.009 16	0.0192	23.2	4.87	-0.0265
b267	-9.2	0.121	11.6	-59.1	0.0295	0.535	72.6
b277	0.001 43	70	-0.006 57	-0.02	-7.5	36.4	-0.0217
b333	0.000 617	-0.0005	58.5	-0.002 02	0.003 16	0.000 402	0.004 16
b334	1.21	0	-0.006 48	67	-0.003 99	0.003 73	4.26
b335	0.001 61	-28.9	0.009 64	-0.004 11	96.5	3.74	0.011
b336	-0.0036	-2.01	-0.000 215	0.002 01	3.72	145	-0.004 39
b337	8.21	-0.002 74	0.0113	4.26	0.0106	-0.004 83	156
b344	0	0.002 94	67	0.001 08	0.005 33	-0.000 892	-0.007 72
b345	0.009 29	-7.9	-0.0623	-0.089	10.9	-16.8	-0.0892
b346	-0.0278	37.8	-0.0846	-0.116	-16.8	2	0.0116
b347	0.006 47	0.0126	8.55	0.122	0.001 04	-0.001 7	-0.208
b355	5.3	-0.008 47	96.5	5.51	0.028	-0.0255	71.2
b356	-9.82	0.0311	7.38	-16.9	-0.134	-0.235	-19.5
b357	-0.0299	-65.1	0.005 07	0.006 18	143	-19.5	-0.193
b366	-1.73	0.0104	145	1.16	-0.0114	-0.097	-12.7
b367	-0.0406	11.6	0.0688	-0.0194	-19.6	-25.1	-0.472
b377	0.0107	-0.007 93	156	0.0176	0.008 23	-0.0476	0.137
b444	0.767	0.000 402	0.000 369	81.4	-0.003 72	0.0116	-7.64
b445	-0.001 48	34.5	0.005 03	-0.0106	112	41	0.0106
b446	0.002 54	21.2	-0.003 15	0.0327	40.9	192	-0.0431
b447	-20.1	0.003 05	-0.007 74	-22.9	0.0118	-0.0465	253
b455	1.66	-0.008 14	5.52	112	-0.008 63	-0.0149	-9.73
b456	-8.43	-0.114	-16.9	81.7	-0.224	-0.459	-80.8
b457	0.0719	-26.9	-0.004 88	0.178	-19.3	-80.8	-0.367
b466	9.98	0.0206	1.16	192	0.0156	0.393	-103
b467	0.195	-59.1	-0.002 07	0.455	-80.9	-205	-0.59
b477	0.215	-0.0217	0.0231	252	-0.043	0.003 34	0.049
b555	-0.000 449	-6.75	0.009 86	-0.002 93	76.1	-9.91	0.0205
b556	0.001 39	10.4	-0.0263	-0.0158	-29.7	158	-0.0479
b557	2.57	-0.003 12	71.3	-9.74	0.0581	-0.0474	240
b566	0.005 79	23.2	-0.0138	0.0161	158	-0.405	-0.0349
b567	-17.9	0.118	-19.6	-81.1	-0.0376	0.243	-0.642
b577	0.004 84	-7.5	0.006 27	-0.0436	240	-0.186	-0.007 17
b666	-0.0145	1.63	-0.0311	0.139	-0.136	357	-0.105
b667	0.147	-0.0237	-12.7	-103	-0.0374	-0.317	406
b677	-0.005 76	36.6	-0.0549	0.001 93	-0.251	406	0.145
b777	-0.0396	-0.006 22	0.0474	0.0102	-0.001 17	0.0459	295



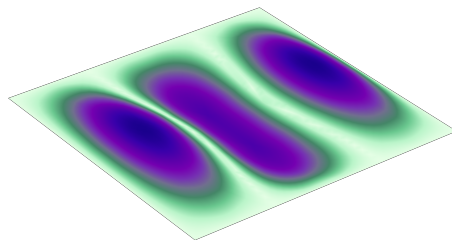
(a) 1st mode



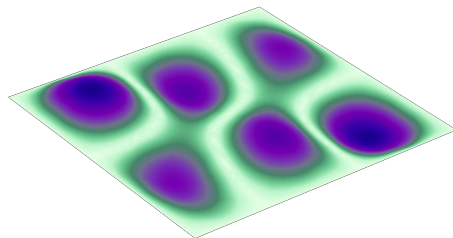
(b) 2nd mode



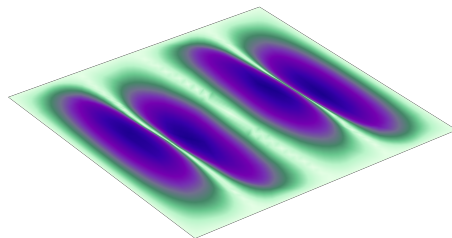
(c) 4th mode



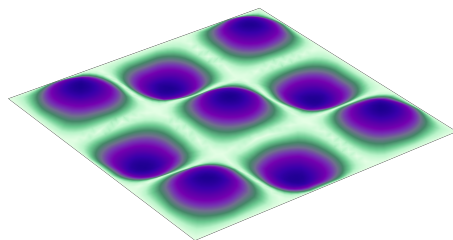
(d) 5th mode



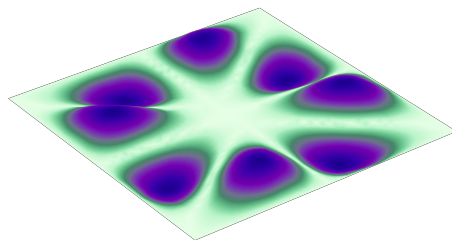
(e) 7th mode



(f) 9th mode



(g) 11th mode



(h) 12th mode

Supplementary Figure 2: Eigenmodes of a square membrane resonator

2.3 Reduced-order model parameters for a string resonator

Reduced-order model of an ideal string resonator is based on an FE model constructed in COMSOL, considering pinned boundary condition with truss elements. The description of model parameters, scaling values and linear modal parameters can be found in Supplementary Tables 5, 9 and 10. We construct the model using the first three out-of-plane and first three in-plane modes of the structure. Nonlinear coefficients can be found in the Supplementary Tables 11 and 12.

Supplementary Table 9: Scaling values for a string resonator

m_t	$k_{0\text{out}}$	Linear			Nonlinear	
		$k_{0\text{in}}$	$\omega_{0\text{out}}$	$\omega_{0\text{in}}$	a_{dim}	b_{dim}
ρAL	$\frac{\sigma A}{L}$	$\frac{EA}{L}$	$\frac{1}{2L}\sqrt{\frac{\sigma}{\rho}}$	$\frac{1}{L}\sqrt{\frac{E}{\rho}}$	$\frac{EA}{L^2}$	$\frac{EA}{L^3}$

Supplementary Table 10: Dimensionless linear modal values of a string resonator. Eigenfrequencies are normalized w.r.t. the fundamental mode (ω_1). Note that Eq. 4, Eq. 5 & Eq. 6 describe in-plane modes.

	Eq. 1	Eq. 2	Eq. 3	Eq. 4	Eq. 5	Eq. 6
m/m_t	0.5	0.5	0.499	0.5	0.501	0.497
k/k_0	4.93	19.7	44.4	4.97	19.9	44.6
ω/ω_1	1	2	3	23.6	47.2	70.9

Supplementary Table 11: Quadratic nonlinear coefficients for a string resonator modelled with modes: first three out-of-plane modes (correspond to 1,2,3 in the table) and first three in-plane modes (correspond to 4,5,6 in the table)

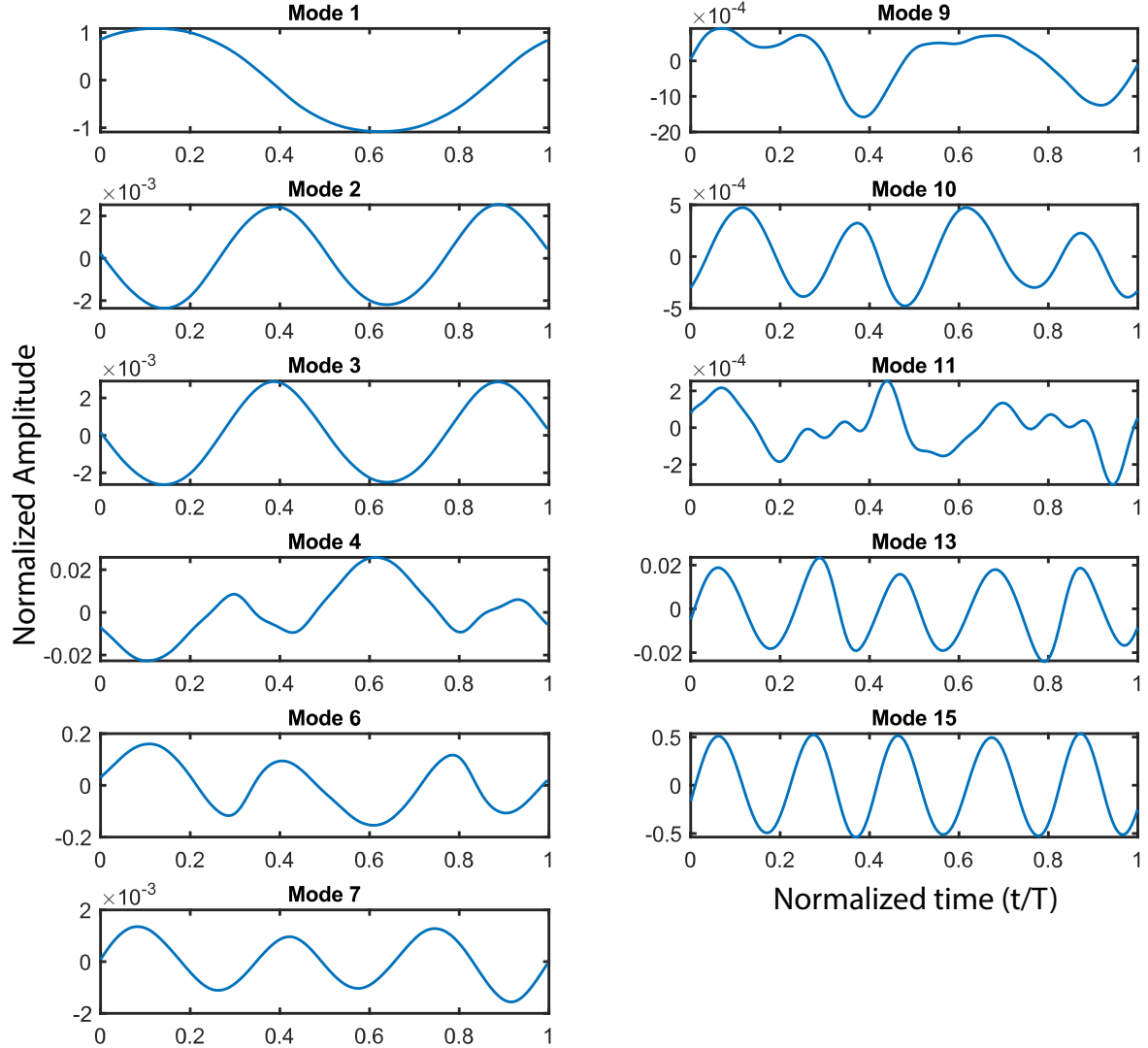
	Eq. 1	Eq. 2	Eq. 3	Eq. 4	Eq. 5	Eq. 6
a_{11}	0	0	0	7.75	-0.000 153	-0.0014
a_{12}	0	0	0	0	0	0
a_{13}	0	0	0	46.5	-93.1	0.006 46
a_{14}	15.5	0	46.5	0	0	0
a_{15}	-0.000 152	0	-93.1	0	0	0
a_{16}	-0.001 32	0	0.008 06	0	0	0
a_{22}	0	0	0	0	-62.1	0
a_{23}	0	0	0	0	0	0
a_{24}	0	0	0	0	0	0
a_{25}	0	-124	0	0	0	0
a_{26}	0	0	0	0	0	0
a_{33}	0	0	0	0.000 349	-0.001 73	-209
a_{34}	46.5	0	-0.001 16	0	0	0
a_{35}	-93.1	0	-0.001 73	0	0	0
a_{36}	-0.001 08	0	-418	0	0	0
a_{44}	0	0	0	0	-186	0
a_{45}	0	0	0	-372	0	1.12×10^3
a_{46}	0	0	0	0	1.12×10^3	0
a_{55}	0	0	0	0	0	0
a_{56}	0	0	0	1.12×10^3	0	0.0162
a_{66}	0	0	0	0	-0.0111	0

Supplementary Table 12: Cubic nonlinear coefficients for a string resonator modelled with modes: first three out-of-plane modes (that correspond to 1, 2, 3 in the table) and first three in-plane modes (that correspond to 4, 5, 6 in the table)

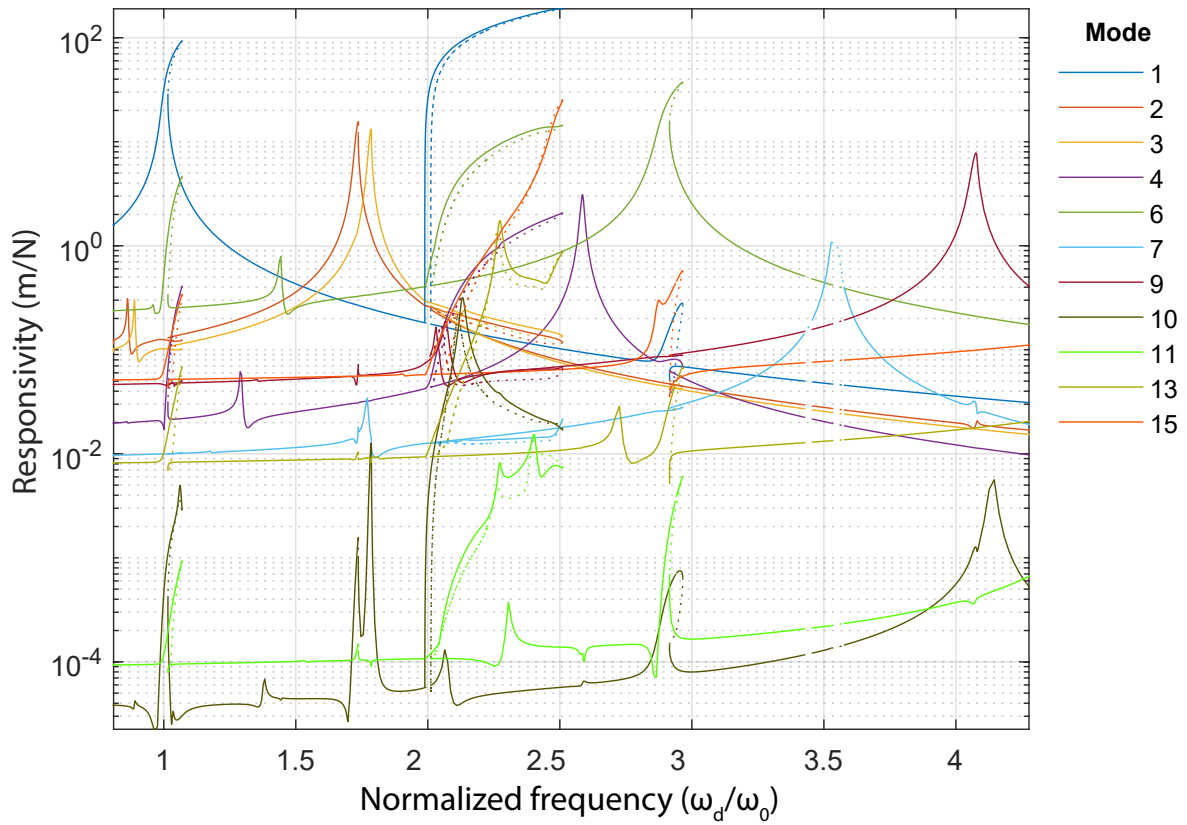
	Eq. 1	Eq. 2	Eq. 3	Eq. 4	Eq. 5	Eq. 6
b_{111}	18.3	0	18.3	0	0	0
b_{112}	0	146	0	0	0	0
b_{113}	54.8	0	328	0	0	0
b_{114}	0	0	0	48.7	-48.8	0.00533
b_{115}	0	0	0	-48.8	195	146
b_{116}	0	0	0	0.00403	146	437
b_{122}	146	0	219	0	0	0
b_{123}	0	438	0	0	0	0
b_{124}	0	0	0	0	0	0
b_{125}	0	0	0	0	0	0
b_{126}	0	0	0	0	0	0
b_{133}	328	0	-0.0227	0	0	0
b_{134}	0	0	0	146	-292	-437
b_{135}	0	0	0	-292	-0.00655	876
b_{136}	0	0	0	-437	876	-0.0632
b_{144}	48.7	0	73	0	0	0
b_{145}	-97.5	0	-292	0	0	0
b_{146}	0.00747	0	-437	0	0	0
b_{155}	195	0	-0.00386	0	0	0
b_{156}	292	0	876	0	0	0
b_{166}	437	0	-0.0141	0	0	0
b_{222}	0	292	0	0	0	0
b_{223}	219	0	1.31×10^3	0	0	0
b_{224}	0	0	0	292	0	-292
b_{225}	0	0	0	0	781	0
b_{226}	0	0	0	-292	0	1.75×10^3
b_{233}	0	1.31×10^3	0	0	0	0
b_{234}	0	0	0	0	0	0
b_{235}	0	0	0	0	0	0
b_{236}	0	0	0	0	0	0
b_{244}	0	292	0	0	0	0
b_{245}	0	0	0	0	0	0
b_{246}	0	-583	0	0	0	0
b_{255}	0	781	0	0	0	0
b_{256}	0	0	0	0	0	0
b_{266}	0	1.75×10^3	0	0	0	0
b_{333}	0.00417	0	1.48×10^3	0	0	0
b_{334}	0	0	0	438	-439	0.0182
b_{335}	0	0	0	-439	1.76×10^3	-0.0141
b_{336}	0	0	0	0.00627	0.00105	3.93×10^3
b_{344}	73	0	438	0	0	0
b_{345}	-292	0	-877	0	0	0
b_{346}	-437	0	0.0373	0	0	0
b_{355}	0.000582	0	1.76×10^3	0	0	0
b_{356}	876	0	-0.0161	0	0	0
b_{366}	-0.011	0	3.93×10^3	0	0	0
b_{444}	0	0	0	292	0	-290
b_{445}	0	0	0	0	2.34×10^3	0
b_{446}	0	0	0	-875	0	5.24×10^3
b_{455}	0	0	0	2.34×10^3	0	-3.51×10^3
b_{456}	0	0	0	0	-7.02×10^3	0
b_{466}	0	0	0	5.24×10^3	0	0.502
b_{555}	0	0	0	0	4.7×10^3	0
b_{556}	0	0	0	-3.51×10^3	0	2.1×10^4
b_{566}	0	0	0	0	2.1×10^4	0
b_{666}	0	0	0	0.132	0	2.35×10^4

3 Dynamic response of the graphene drum during internal resonance

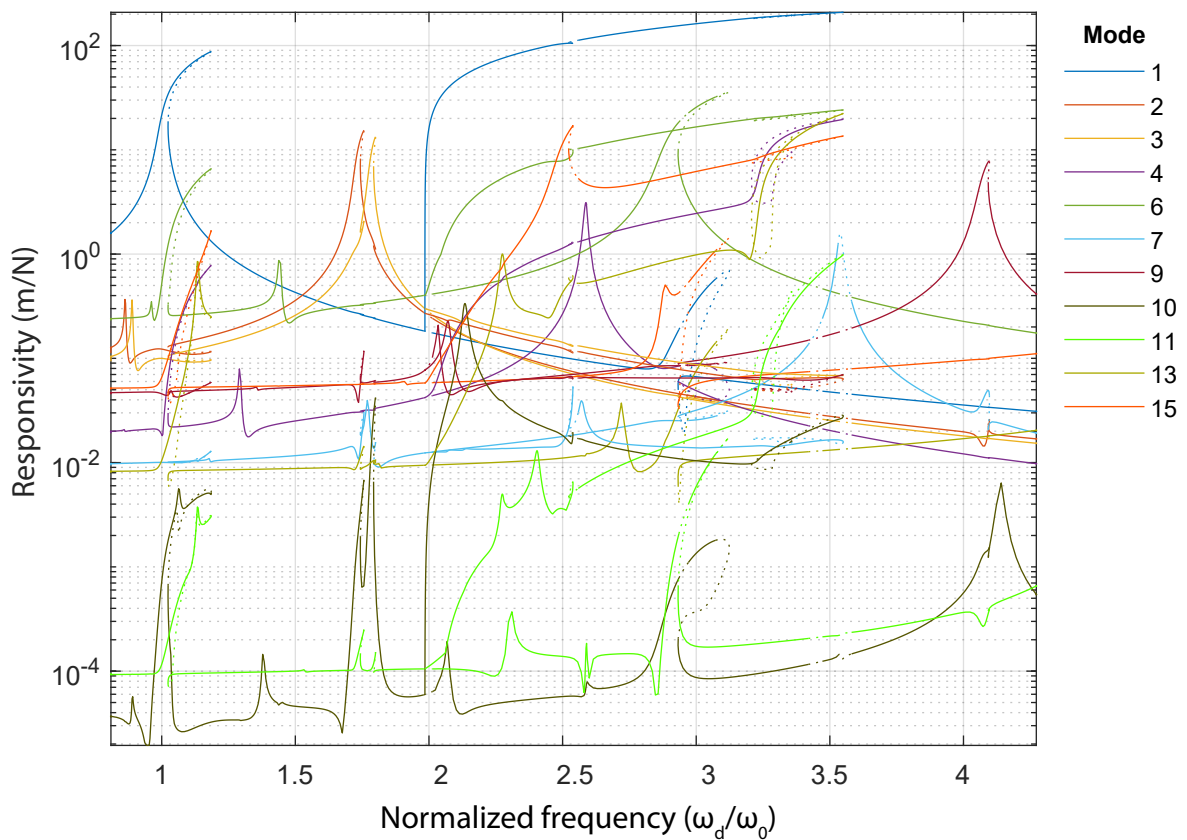
In the main text, experiments were displayed where complex nonlinear phenomena occur, one of which is internal resonance caused by the interaction of the parametric resonance of the first mode with other modes of vibration. In the simulations, these observations were replicated. Here, we further investigate this response. In Supplementary Fig. 3, we show the time response of each mode during once cycle of the internal resonance at $\omega_d/\omega_0 = 2.538$. It is possible to observe strong activation of multiple modes. The dominant modes are the first three axisymmetric modes $f_{0,1}$, $f_{0,2}$ and $f_{0,3}$ (mode numbers 1,6,15) together with asymmetric mode $f_{2,1}$ (mode number 4). This is also clear in the overall frequency responses in Supplementary Fig. 4 with all the simulated modes.



Supplementary Figure 3: Time responses of each mode during a period of oscillation for the graphene drum undergoing internal resonance at $\omega_d/\omega_0 = 2.538$.



(a) Simulated modal frequency response for excitation level $\beta = 14.32$ and $\gamma = 2.5$, before the surge.



(b) Simulated modal frequency response for excitation level $\beta = 26.22$ and $\gamma = 3.2$, after the surge.

Supplementary Figure 4: Global multi-mode frequency responses of the simulated graphene drum

References

- [1] M. Amabili. *Nonlinear Vibrations and Stability of Shells and Plates*. Jan 2010.
- [2] D. Davidovikj, F. Alijani, S. J. Cartamil-Bueno, H. S. J. van der Zant, M. Amabili, and P. G. Steeneken. Nonlinear dynamic characterization of two-dimensional materials. *Nat Commun*, 8:1253, 2017.
- [3] A. Keşkekler, H. Arjmandi-Tash, P. G. Steeneken, and F. Alijani. Symmetry-breaking-induced frequency combs in graphene resonators. *Nano Letters*, 22(15):6048–6054, Aug 2022.
- [4] A. A. Muravyov and S. A. Rizzi. Determination of nonlinear stiffness with application to random vibration of geometrically nonlinear structures. *Computers & Structures*, 81(15):1513 – 1523, 2003.